Arctic Cloud Microphysics Retrievals from Surface-Based Remote Sensors at SHEBA

MATTHEW D. SHUPE

Cooperative Institute for Research in Environmental Sciences, University of Colorado, and NOAA Environmental Technology Laboratory, Boulder, Colorado

TANEIL UTTAL

NOAA Environmental Technology Laboratory, Boulder, Colorado

SERGEY Y. MATROSOV

Cooperative Institute for Research in Environmental Sciences, University of Colorado, and NOAA Environmental Technology Laboratory, Boulder, Colorado

(Manuscript received 3 August 2004, in final form 5 May 2005)

ABSTRACT

An operational suite of ground-based, remote sensing retrievals for producing cloud microphysical properties is described, assessed, and applied to 1 yr of observations in the Arctic. All measurements were made in support of the Surface Heat Budget of the Arctic (SHEBA) program and First International Satellite Cloud Climatology Project Regional Experiment (FIRE) Arctic Clouds Experiment (ACE) in 1997–98. Retrieval techniques and cloud-type classifications are based on measurements from a vertically pointing 35-GHz Doppler radar, microwave and infrared radiometers, and radiosondes. The retrieval methods are assessed using aircraft in situ measurements from a limited set of case studies and by intercomparison of multiple retrievals for the same parameters. In all-liquid clouds, retrieved droplet effective radii R_e have an uncertainty of up to 32% and liquid water contents (LWC) have an uncertainty of 49%–72%. In all-ice clouds, ice particle mean sizes D_{mean} can be retrieved with an uncertainty of 26%–46% while retrieved ice water contents (IWC) have an uncertainty of 62%–100%. In general, radar-only, regionally tuned empirical power-law retrievals were best suited among the tested retrieval algorithms for operational cloud monitoring at SHEBA because of their wide applicability, ease of use, and reasonable statistical accuracy. More complex multisensor techniques provided a moderate improvement in accuracy for specific case studies and were useful for deriving location-specific coefficients for the empirical retrievals but were not as frequently applicable as the single sensor methods because of various limitations. During the yearlong SHEBA program, all-liquid clouds were identified 19% of the time and were characterized by an annual average droplet R_e of 6.5 μm, LWC of 0.10 g m^{-3}, and liquid water path of 45 g m^{-2}. All-ice clouds were identified 38% of the time with an annual average particle D_{mean} of 73 μm, IWC of 0.014 g m^{-3}, and ice water path of 30 g m^{-2}.

1. Introduction

Ground-based remote sensing of cloud properties has become an increasingly important field, particularly because retrieval algorithms used from the ground are now being modified and prepared for widespread use from space (Stephens et al. 2002). Cloud radars and/or lidars have been used to derive quantities such as ice cloud microphysical properties (e.g., Sassen 1987; Matrosov et al. 1992; Atlas et al. 1995; Mace et al. 1998; Donovon and van Lammeren 2001; Wang and Sassen 2002), liquid cloud microphysical properties (e.g., Liao and Sassen 1994; Frisch et al. 1995; Fox and Illingworth 1997; Dong et al. 1997; Lohnert et al. 2001; McFarlane et al. 2002), and cloud optical properties (Matrosov et al. 2002, 2003; Hogan et al. 2003). Some methods have been utilized to create continuous records of cloud properties at specific sites (Dong et al. 2000; Shupe et al. 2001; Hogan et al. 2003) and to validate satellite cloud retrievals (Dong et al. 2002; Stephens et al. 2002).

Corresponding author address: Matthew Shupe, CIRES/NOAA/ETL, R/ET6, 325 Broadway, Boulder, CO 80305.
E-mail: matthew.shupe@noaa.gov

Although various studies have described the uncertainties associated with specific retrieval techniques (e.g., Liu and Illingworth 2000; Frisch et al. 2002; Mace et al. 2002; Matrosov et al. 2002; Sassen et al. 2002), few intercomparisons have been performed that would ensure consistency between results. For these reasons, it is important to assess the level of certainty and consistency with which ground-based retrievals can be applied.

Long-term, continuous records of vertically resolved cloud properties are necessary for monitoring the evolution of clouds in response to climate change and are needed to better characterize cloud properties/processes so that they can be more accurately modeled. At present, the use of ground-based remote sensors to produce these records requires less manpower, needs fewer financial resources, and provides wider temporal coverage than do aircraft in situ cloud measurements. Also, although in situ measurements are often considered ground truth, the uncertainties associated with these measurements, particularly in ice clouds, are high (e.g., Larsen et al. 1998; Gayet et al. 2002). Thus, remote sensor records provide important information that is in many ways complementary to aircraft observations. Satellite passive retrievals offer extensive spatial coverage but do not typically provide vertically resolved cloud properties and have difficulties related to scene/cloud classification (e.g., Rossow et al. 1993), subpixel cloud variability (e.g., Wielicki and Parker 1992), and vertical cloud placement (e.g., Frey et al. 1999). Long records of accurate surface-derived cloud properties are needed to assess, validate, and improve satellite retrievals. Additionally, most applications of ground-based retrievals have typically focused on case studies or limited regimes of cloudiness. It is therefore important to establish operational ground-based retrievals that are capable of producing long records of cloud properties at specific locations.

The objectives of this study are to describe an operational framework to produce continuous retrievals of cloud properties from a suite of surface-based instruments, and to assess the uncertainties of the specific retrieval methods. This study is limited to a subset of cloud microphysical retrieval techniques developed at the National Oceanic and Atmospheric Administration (NOAA) Environmental Technology Laboratory (ETL) that were applied to an annual cycle of remote observations by a radar and various radiometers in the Arctic. The observational dataset is from the Surface Heat Budget of the Arctic (SHEBA) program (Uttal et al. 2002), which took place in the Beaufort and Chukchi Seas from October 1997 to October 1998. Aircraft data from the collaborating First International Satellite Cloud Climatology Project (ISCCP) Regional Experiment (FIRE) Arctic Clouds Experiment (ACE; Curry at al. 2000), which took place during the spring/summer of 1998 near SHEBA, are used to assess the ground-based retrievals for a limited set of case studies. A broader comparison of retrieval techniques based on 1 yr of retrieval results is also performed. Some results from an earlier version of this retrieval framework for April through July at SHEBA have been presented in Shupe et al. (2001). Here, the retrieval package is extended and modified, and the uncertainties are examined. This package is then utilized to provide a look at single-phase cloud microphysical properties over an annual cycle in the Arctic.

2. Instruments and techniques

a. Instruments

All cloud microphysical retrievals discussed here use measurements from a vertically pointing 35-GHz, millimeter-wavelength cloud radar (MMCR; Moran et al. 1998). The MMCR produces profiles, above its lowest range gate at 105 m, of radar reflectivity Z_e, mean Doppler velocity V_z, and Doppler spectrum width, with 45-m vertical and 10-s temporal resolution. The radar has a detection threshold of -47 dBZ at 5 km above ground level, and a reflectivity uncertainty of <1 dB (K. P. Moran 2004, personal communication).

Radiometric input for two of the cloud retrievals is provided by the microwave radiometer (MWR) and the Atmospheric Emitted Radiance Interferometer (AERI; Knuteson et al. 2004), both of which are operated by the U.S. Department of Energy Atmospheric Radiation Measurement Program at SHEBA. The MWR measures brightness temperatures of downwelling radiation at 23.8 and 31.4 GHz that are used to derive column-integrated amounts of precipitable water vapor and liquid water path (LWP). The data used here were reprocessed to include updated information on the dielectric constants of supercooled liquid water and the absorption of dry air, yielding an LWP uncertainty of about 25 g m^{-2} (Westwater et al. 2001). Prior to 5 December 1997, the MWR dataset suffered from irrecoverable calibration problems and is therefore not used in this study. Sky infrared brightness temperature T_{IR} is calculated from the integrated downwelling IR radiance from the AERI over a 25-cm^{-1} band centered on 900 cm^{-1} (11.1 μm). This band is affected very little by the water vapor continuum in the Arctic atmosphere. The AERI observations ended on 4 July 1998.

Profiles of temperature, humidity, wind speed, and wind direction were measured at SHEBA with a GPS/loran atmospheric-sounding radiosonde system. Sound-

ings were centered on 1200 and 0000 UTC throughout the SHEBA experiment, with additional soundings at 0600 and 1800 UTC during portions of April–July 1998. Temperature profiles used in this study were linearly interpolated to the MMCR's time–height grid.

The 523-nm depolarization and backscatter unattended lidar (Intrieri et al. 2002) was used for cloud-type classification but not for microphysical retrievals. The lidar's depolarization capability provides cloud-phase information that is useful for identifying cloud type.

Aircraft measurements were made near the SHEBA ice camp by the National Center for Atmospheric Research C-130 in May and July (Curry et al. 2000). Microphysical measurements from two King hot-wire probes, a forward-scattering spectrometer probe (FSSP), a particulate volume monitor (PVM), a cloud particle imager (CPI), and a two-dimensional optical array (2DC) cloud probe were utilized in this study. Corrections were applied to the PVM (Laursen 1998) and King probes (K. Laursen 2001, personal communication). Clear-sky biases (nonzero measurements in clear sky) were taken into account on a case-by-case basis. The FSSP total number concentrations are considered to be accurate; however, the FSSP particle sizing is expected to be in error, causing high biases in both the liquid water content and droplet radius (Lawson et al. 2001). Using these data, a cloud is considered to be all liquid if the FSSP number concentration is greater than 5 cm^{-3} and the concentration of particles larger than 200 μm measured by the 2DC is less than 0.1 L^{-1} (Pinto et al. 2001). Raw 1-s data are used to compute all statistical in situ results.

b. Classification method

Prior to the application of cloud retrievals, radar observations of cloud scenes at SHEBA were subjectively classified as all ice, all liquid, mixed phase, or precipitation (rain, snow, or drizzle) using a combination of measurements: reflectivity, mean Doppler velocity, and Doppler spectrum width from the MMCR; LWP derived from the MWR; temperature and humidity profiles from the radiosondes; depolarization ratios from the lidar; and surface observer records. Mixed-phase clouds are defined as cloud layers that contain both liquid and ice. However, this definition does not imply that all portions of clouds classified as mixed phase contain both liquid and ice in the same volume.

The criteria provided in Table 1 were collectively used to guide the classification process. Some criteria were considered to always hold true; others were considered to be moderately flexible, depending upon the collective information from all measurements. For example, only ice hydrometeors exist below −40°C, only liquid hydrometeors exist above 0°C, and all classification types except rain can exist between these temperatures. From the lidar perspective, depolarization ratios of less than ~0.11 indicate liquid droplets and higher ratios indicate ice particles (Sassen 1984; Intrieri et al. 2002). In terms of specific cloud types, ice clouds were identified as having a zero LWP and typically had reflectivities of <0 dBZ and Doppler velocities of <1 m s^{-1}. All-liquid, drizzle-free clouds were characterized by a positive LWP, reflectivities of <−15 dBZ (i.e., Frisch et al. 1995), and Doppler velocities of typically <0.5 m s^{-1}. In contrast to the liquid clouds, mixed-phase, drizzle, and other precipitation cases typically had higher reflectivities and velocities. Drizzle and mixed-phase clouds had similar signatures in the radar Doppler moments; however, the drizzling clouds were typically near or above 0°C, whereas the mixed-phase clouds were always below freezing. The Doppler spectrum width was qualitatively useful for distinguishing mixed-phase from ice clouds. Under mixed-phase con-

TABLE 1. Criteria for cloud-type classification. The criteria in boldface are considered to be always true; the rest are considered to be moderately flexible, depending upon the collective information from all criteria. The asterisk indicates that the specified criterion is fulfilled somewhere throughout the depth of the cloud layer.

	Snow	Ice	Mixed phase	Liquid	Drizzle	Rain
Temperature T (°C)	**<0**	**<0**	**−40 < T < 0**	**>−40**, >−20	**>−40**, >−10	**>0**
	Only ice: T < −40		—		**Only liquid: T > 0**	
Depolarization ratio, lidar	**>0.15**, >0.2	**>0.15**, >0.2	**<0.11* and >0.11***	**<0.11**	<0.11	<0.11
LWP (g m^{-2})	**0**	**0**	**>0**	**>0**	**>0**	**>0**
Reflectivity (dBZ)	>−10	<0	<10	**<−15**	**>−15*** and <10	**Melting layer feature**
Mean Doppler velocity (m s^{-1})	>0.5	$0 < V_z < 1$	$-0.1 < V_z < 1.5$	<0.5	$0 < V_z < 2$	**Melting layer feature**
Spectral width (m s^{-1})	—	<0.4	>0.5*	—	—	**Melting layer feature**

ditions, the Doppler spectrum is often broader, in part because of the difference in fall speeds between liquid droplets and ice particles (Shupe et al. 2004). The association of broadened spectrum widths with mixed-phase conditions has been confirmed with collocated lidar depolarization measurements in many cases during SHEBA (Shupe et al. 2005, manuscript submitted to *J. Atmos. Sci.*). Rain and snow were identified by high Doppler velocities and were distinguished from each other by temperature and by surface observer notes. Rain was also usually associated with a radar bright band, which occurs when falling ice particles melt into raindrops. These general criteria were combined to determine the most likely phase of all clouds observed above the SHEBA site, and the classifications were reviewed multiple times to ensure consistency and accuracy.

An example classification is discussed here for a complex, multilayered, 10-h period on 18 May at SHEBA. The radar reflectivity, mean Doppler velocity, and Doppler spectrum width; lidar depolarization ratio; cloud-type classification mask; and MWR-derived LWP are shown in Fig. 1. Throughout this time period there were three basic types of clouds: high cirrus, midlevel mixed phase, and boundary layer stratus. The early portion of the cirrus layer on this day extended from 3 to 9 km; after about 0300 (all times are in UTC) the layer thinned to the 6–9-km range. The decreases in radar Z_e and V_z with height are often observed in cirrus clouds, indicating smaller particles near the cloud top that grow with depth in the cloud. In the first hour of the day, during which there were no lower-level clouds present, the MWR showed no significant LWP in this ice layer, and lidar depolarization ratio measurements above 0.2 also indicated the presence of ice only. Shortly after 0100 a boundary layer stratus deck of supercooled liquid water topped by a shallow temperature inversion advected over the ice camp. The LWP steadily increased during the rest of the 10-h period. Until about 0520, radar reflectivities above -15 dBZ and lidar depolarization ratios indicating both ice and liquid suggested that ice crystals precipitated from this liquid layer. After 0520 the stratus layer contained no ice precipitation according to the lidar measurements. At about 0440 a midlevel mixed-phase cloud layer was observed by the radar. Mean Doppler velocities in the upper portion of this cloud were, at times, near zero, suggesting small liquid droplets, while lower in the cloud the velocities were much larger, suggesting large ice particles. Wide Doppler spectrum widths, which can indicate the presence of both phases (Shupe et al. 2004, 2005), also suggest that this midlevel cloud was topped by a thin liquid layer with cloud ice extending below the liquid cloud base at about 4 km. In addition, after 0520 the increasing MWR-derived total column LWP is significantly higher than the LWP derived for the lower cloud layer from radar measurements (dots in Fig. 1f; see below), suggesting that liquid water is present somewhere in the higher cloud layers.

c. Retrieval methods

The microphysical retrieval methods utilized in the operational retrieval system are briefly outlined here and are summarized in Table 2. Some methods have been added and/or modified since their application by Shupe et al. (2001). For more details on the theoretical background and development of each technique, see the provided references. All retrieval results have 45-m vertical and 1-min temporal resolution.

Retrievals of liquid water content (LWC) and droplet effective radius R_e are performed using two techniques. The radar-radiometer technique (Frisch et al. 1995, 1998, hereinafter jointly referred to as FRI) uses the radar Z_e profile and the MWR-derived LWP to constrain the liquid water profile throughout liquid clouds. This method is only applicable when all of the column liquid is contained within all-liquid, nondrizzling cloud layers and therefore cannot be used when mixed-phase or precipitating clouds are present or a portion of cloud cover is below the lowest radar range gate (e.g., the method is not applicable for the liquid cloud after 0520 in Fig. 1).

A second, radar-only, liquid cloud retrieval (referred to as ROL) is based on a set of power-law relationships between Z_e and liquid cloud parameters (Table 2). The coefficients of these relationships assume a fixed droplet concentration N_l and logarithmic width σ of the assumed lognormal droplet size distribution (DSD) that were obtained from episodic C-130 aircraft flights in all-liquid clouds during FIRE ACE. Here, the mean in situ value of $\sigma = 0.30$ and the median value of $N_l = 75$ cm^{-3} are assumed, because the distribution of N_l is strongly skewed. The assumed N_l is reasonable, considering that most in situ observations in the Beaufort Sea region have shown concentrations less than 100 cm^{-3} (Hobbs and Rangno 1998; Gultepe et al. 2000; Pinto et al. 2001) and that the averaged marine stratus N_l, from a review of global observations, is 74 cm^{-3} (Miles et al. 2000). The retrievals are not very sensitive to the specification of σ and are moderately sensitive to the specification of N_l. Varying σ and N_l to the 25th or 75th percentiles of the in situ observations would change LWC retrievals by $\pm 10\%$ and $\pm 25\%$, respectively, and R_e retrievals by $\pm 1\%$ and $\pm 8\%$, respectively. The ROL

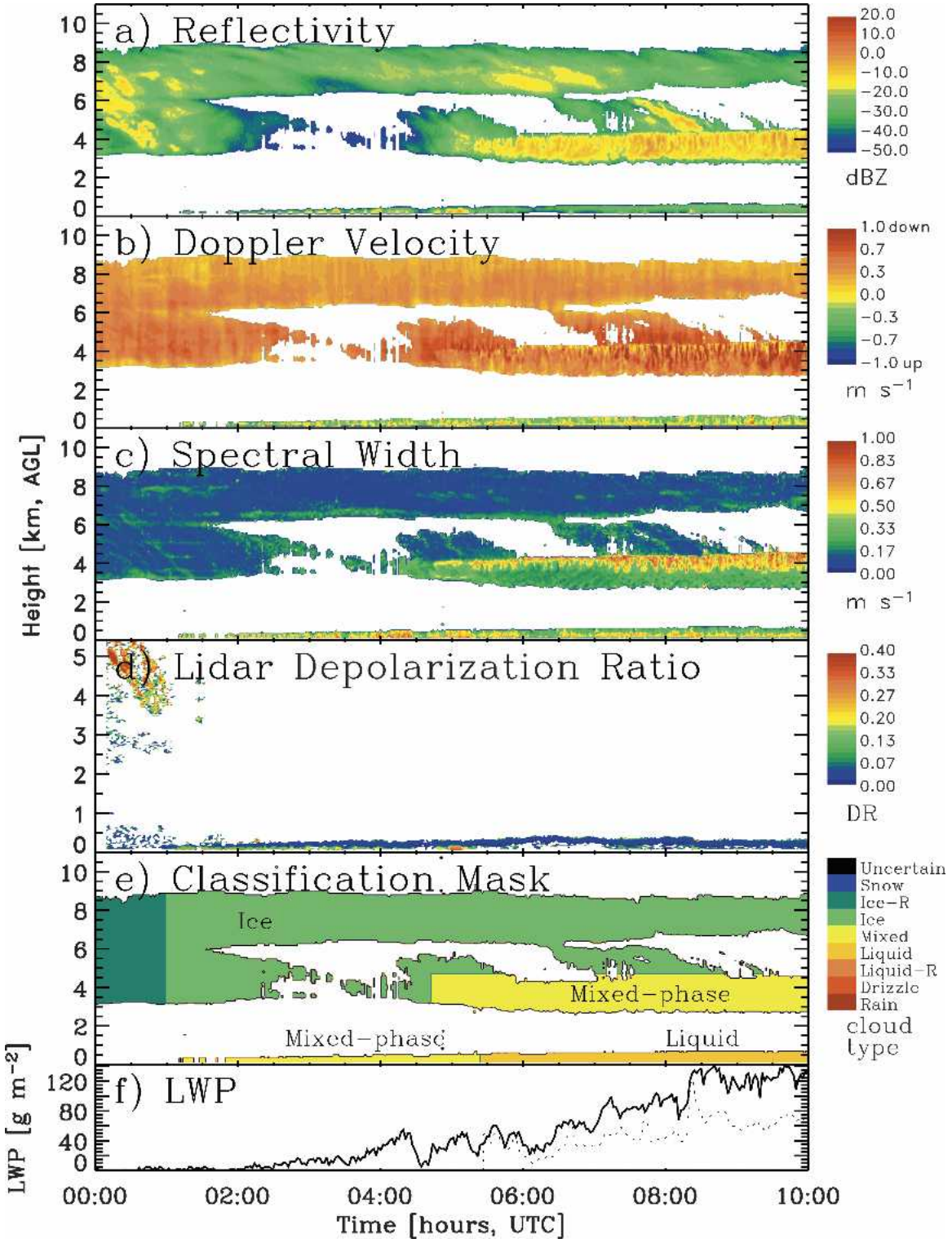

FIG. 1. Radar (a) reflectivity, (b) mean Doppler velocity, and (c) Doppler spectrum width; (d) lidar depolarization ratio; (e) cloud-type classification mask; and (f) microwave radiometer–derived total LWP (line) and radar-derived LWP for the lower cloud layer (dots) on 18 May 1998. The vertical axis covers a different range in (d).

TABLE 2. Ground-based remote sensing cloud microphysical retrieval techniques applied to SHEBA observations. The following standard units are used: R_e, D_o, and D_{mean}: μm; LWC and IWC: g m^{-3}; N_l: cm^{-3}; Z_e: mm^6 m^{-3}.

Characteristic	Cloud liquid methods		Cloud ice methods	
Abbreviation, text reference	FRI Frisch et al. (1995, 1998)	ROL Frisch et al. (2002)	M99 Matrosov (1999)	M02 Matrosov et al. (2002)	ROI Details in section 2c
Cloud types	All liquid, fully observed, no mixed phase in column	All liquid	All ice, no liquid in column	All ice or the ice component of mixed phase, no vertical air motion residual	All ice or the ice component of mixed phase
Input measurements	Z_e, LWP	Z_e	Z_e, T_{IR}, PWV, T_{sonde}	Z_e, V_z	Z_e
Temporal resolution	1 min	1 min	1 min	20-min running averages at 1 min	1 min
Assumed DSD/PSD	Lognormal	Lognormal	Exponential	Exponential	Exponential
Equations	$N_l = N_l(\text{LWP}, Z_e)$, constant with height	LWC $= cZ_e^{1/2}$, $R_e = dZ_e^{1/6}$	IWC $= aZ_e^b$, $D_o = (Z_e/\text{IWC}/G)^{1/3}$, $G = (8 \times 10^{-5})(D_o)^{-1.1}$	$D_o = D_o(V_z)$*, IWC $= Z_e/D_o^3/G$, $G = (8 \times 10^{-5})(D_o)^{-1.1}$	IWC $= aZ_e^b$, $D_o = 143a^{-0.53}Z_e^{0.53(1-b)}$
Fixed coefficients, parameters	$\sigma = 0.30$	$c = \pi/6 \exp(-4.5\sigma^2)N_l^{1/2} = 3.0$, $d = 50 \exp(-0.5\sigma^2)N_l^{-1/6} = 23$, $\sigma = 0.30$, $N_l = 75$	$a = a(T_{\text{IR}})$*, $b = b(h)$*, $D_o = 3.54D_{\text{mean}}$	$D_o = 3.54D_{\text{mean}}$	$a = a(\text{time})$*, $b = 0.63$, $D_o = 3.54D_{\text{mean}}$

* Further details provided in section 2c.

technique was performed in all liquid-only clouds, including all clouds to which the FRI technique was also applied.

Ice cloud retrievals are generally less robust than liquid retrievals because of the complexities introduced by the variety of ice particle habits and their scattering properties. Ice water content (IWC) and particle physical characteristic size (the median volume diameter D_o) retrievals are based on the power-law relationship IWC $= aZ_e^b$ (IWC: g m^{-3}; Z_e: mm^6 m^{-3}). By incorporating the AERI-derived T_{IR} to estimate the cloud optical depth, Matrosov (1999, hereinafter M99) proposed a method to tune the a coefficient to a given cloud profile. M99 also suggested a vertical profile of the b exponent that decreases linearly from 0.7 at cloud base to 0.55 at cloud top. For a measured Z_e and an estimated IWC, D_o is then derived using a relationship among D_o, IWC, and Z_e (M99), which depends on the particle density–size relationship (e.g., Brown and Francis 1995) and the assumed exponential shape of the particle size distribution (PSD). For the exponential PSD, the mean diameter, which is the physical size reported here, is related to D_o by the relation $D_{\text{mean}} \approx D_o/3.54$. Because this technique uses downwelling IR radiances, it is only useful when there is no liquid in the atmospheric column that would radiometrically obscure the brightness temperatures of the ice cloud (e.g., this method is applicable to the ice cloud before, but not after, 0100 in Fig. 1).

A second ice cloud retrieval utilizes radar Z_e and V_z alone (Matrosov et al. 2002, hereinafter M02). According to this scheme, by averaging V_z for 15–30 min (here a 20-min running average is used) the vertical air motion is minimized and the residual approximates the ice particle reflectivity-weighted fall speed. Here, D_o is calculated from the estimated fall speed using a third-order polynomial relationship, and IWC is subsequently determined from the relation among Z_e, IWC, and D_o (M99). A major source of uncertainty in this technique was introduced by small movements of the SHEBA ship that put the radar slightly out of vertical alignment and introduced small V_z contaminations from the horizontal winds. No corrections have been made here because any correction would require interpolating variable radiosonde winds to the radar time–height grid. An analysis of the radar misalignment for time periods coincident with a radiosonde profile showed that most velocity errors caused by the horizontal winds were less than ± 15 cm s^{-1}, with a slight tendency toward a decrease in fall speed that would cause the method to underestimate D_o. A lower limit of 10 cm s^{-1} was placed on the velocity data used for this retrieval.

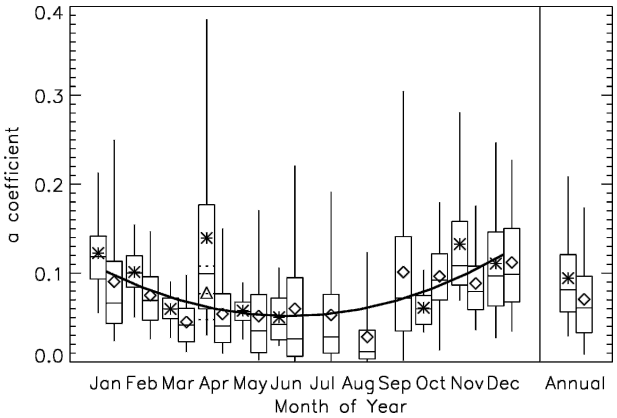

FIG. 2. Monthly statistics of the *a* coefficient derived directly from the M99 method (stars) and indirectly from the M02 method (diamonds) and a polynomial fit to the monthly mean values (thick line). The box-and-whisker plots represent the 5th, 25th, 50th, 75th, and 95th percentiles and show the mean as a symbol. The M99 results in Apr are also shown if one spurious case is removed from the data. Units of *a* are such that IWC is in grams per cubic meter and Z_e is in millimeters to the sixth power per cubic meter in IWC = aZ_e^b.

Last, a radar-only ice cloud retrieval (referred to as ROI) utilizes the same retrieval relationships as M99, albeit with parameterized coefficients. The *b* coefficient for this retrieval takes the average value suggested by M99 (0.63). The *a* coefficient is specified by a polynomial fit to monthly averaged values of *a* determined using two independent approaches; *a* was derived directly from the M99 technique and by reverse calculation from the M02 IWC results. Both approaches produced a consistent annual trend of monthly averaged *a* coefficients with a minimum in the summer and a maximum in the winter (Fig. 2). This trend is likely tied to the annual variation of ice particle sizes and/or densities (i.e., larger sizes in the summer) but may also be affected by optical depth and temperature. Although not tuned to a given cloud scene, the *a* coefficient specified in this manner is appropriate for clouds observed in the SHEBA region and is expected to be superior to any fixed a priori coefficient that would not capture the annual variation of this parameter. However, this specification of *a* may not be appropriate for other geographic locations. The annual mean *a* coefficient at SHEBA was between 0.09 (M99) and 0.07 (M02) and is likely closer to 0.07 because the M99 results do not cover the summer months.

3. Liquid retrieval assessment

Liquid cloud retrieval techniques are first assessed with episodic aircraft measurements made as part of the FIRE ACE program. A broader comparison of retrieval techniques over the full period of operation at SHEBA is then used to understand the performance of the retrievals with respect to each other. Theoretical errors are also explored, and a discussion of the retrieval methods is provided. The bias and relative standard difference (RSD) between two datasets are given by Matrosov et al. (2002), where the RSD is specifically defined as

$$(\mathrm{RSD})^2 = \frac{4}{N}\sum_{i}^{N}(x_i - y_i)^2(x_i + y_i)^{-2}.$$

a. Comparisons between retrieval and in situ measurements

Two methods for assessing the ground-based retrievals by comparison with FIRE ACE aircraft measurements are explored. The first includes direct case-study comparisons, which can be difficult given spatial cloud inhomogeneity, the widely differing methods for measuring or calculating the various parameters, and the dearth of available cases for comparison. The second, and potentially more informative, method compares statistics of microphysical parameters over time periods when aircraft were measuring clouds near the SHEBA ship.

On 18 May, the C-130 flew vertical profiles and horizontal legs through a stratus layer extending from 200 to 470 m that persisted above the SHEBA site for nearly 30 h. Profile comparisons of LWC and R_e at 2129 are shown in Figs. 3a and 3b. Because the aircraft profile was made at some distance from the ship and took a few minutes to complete, radar retrievals were averaged over 10 min to capture the temporal (and thereby spatial) cloud variability over the SHEBA site; the standard deviation of retrieval results over the 10-min period is also plotted. Mean values of the LWC profiles from the PVM, King probe, and retrievals (Fig. 3) all agree to within 27% at worst, and the retrievals tend to overestimate the LWC near cloud base. The radar's 45-m height resolution and 10-min averaging for this case both tend to smooth out variability on the scales observed by the aircraft near cloud top. The R_e comparison (Fig. 3b) shows that the retrievals follow a profile shape similar to that of the PVM R_e but are $\sim$2 μm larger. The average N_l and σ from the FSSP for this profile were 83 cm^{-3} and 0.25, both of which are moderately different from the values assumed in the operational ROL retrieval.

A comparison of five horizontal flight legs from 2230 to 2330 on this day is also shown in Fig. 3. In this com-

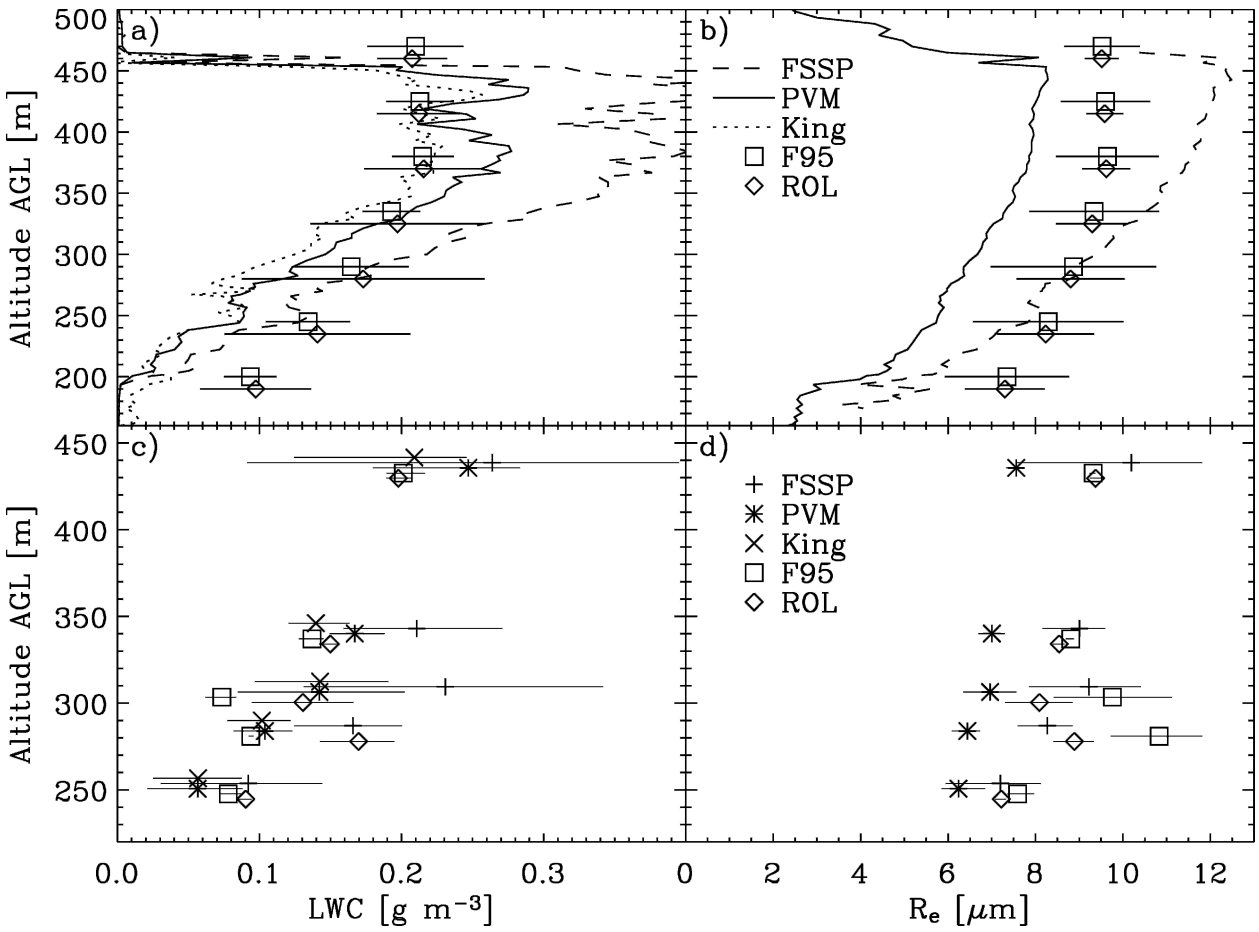

FIG. 3. Cloud property comparisons of in situ measurements and radar-based retrievals during a C-130 flight on 18 May 1998. (top) Profiles of (a) LWC and (b) R_e for an aircraft decent from 2129 to 2131. The standard deviations of retrieval results over the surrounding 10-min time period are given as horizontal lines. Profile-mean values are (a) FSSP: 0.243, PVM: 0.164, King: 0.140, FRI: 0.175, and ROL: 0.178 g m^{-3} and (b) FSSP: 9.6, PVM: 6.7, FRI: 9.0, and ROL: 8.9 μm. (bottom) Comparisons of (c) LWC and (d) R_e for a collection of five horizontal flight legs at different heights from 2230 to 2330. The mean value for each dataset during each leg is given as a symbol, and the range of observations over the leg is given as a horizontal line. Statistics for this comparison are provided in Table 3.

parison, only aircraft data within 5 km of the vertical radar beam are considered. Retrieval results are derived for the time–height of each in situ observation. For each flight leg, the mean value from each instrument or retrieval method is given as a symbol in Figs. 3c and 3d, and the range of observations during the leg is expressed as a horizontal bar. The similarity of these values to those discussed in the previous case (1–2 h earlier) indicates relative temporal, and thus spatial, cloud homogeneity on this day. A statistical analysis of the 724 points that compose this comparison (Table 3) shows that the retrievals have an RSD from the in situ measurements of 44%–49% for LWC and 21%–32% for R_e, with the ROL method showing somewhat better agreement with in situ measurements than does the FRI method.

To complement this case study, further information is derived from a longer-term statistical comparison. Aircraft measurements were compiled for five days that contained persistent and fairly homogeneous all-

TABLE 3. Statistical comparison of retrieval results with in situ observations for five horizontal flight legs (724 points) from 2230 to 2330 18 May 1998. In situ data from the FSSP are not included because these values are suspect (Lawson et al. 2001). All values are in percent.

	PVM–FRI	PVM–ROL	King–FRI	King–ROL	FRI–ROL
LWC, RSD	49	47	47	44	32
LWC, bias	15	−12	9	−18	−6
R_e, RSD	32	21	—	—	12
R_e, bias	−28	−19	—	—	6

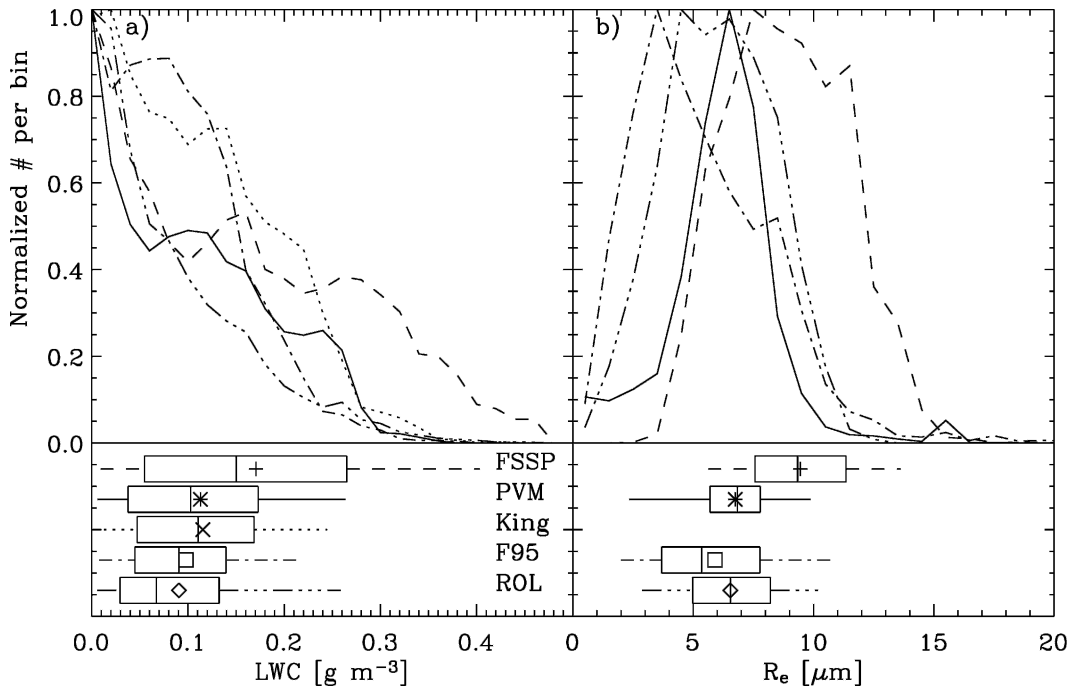

FIG. 4. Distributions of observed and retrieved (a) LWC and (b) R_e from 5 days during which the C-130 was sampling all-liquid clouds. In situ observations were for all measurements in all-liquid clouds within 50 km of the SHEBA site. The retrieval data are for all-liquid clouds observed by the radar during the time periods that the aircraft was sampling within the 50-km range but not necessarily for the same clouds as sampled by the aircraft. The box-and-whiskers plots summarize the data by providing the 5th, 25th, 50th, 75th, and 95th percentiles, and the mean is given as a symbol.

liquid clouds in which the C-130 made measurements: 15, 18, and 27 May and 23 and 29 July. For comparison, retrieval data were compiled for all-liquid clouds observed during the same time periods that the aircraft was sampling in the SHEBA area, although not necessarily in the same clouds at the same times. This comparison dataset includes ~8 h of observations that consist of ~4500 points from the retrievals and more than 10 000 aircraft observations. Results from these comparison cases are summarized in Fig. 4. Because the agreement between the PVM and King probes is good and the FSSP measurements are likely in error, a mean in situ LWC of 0.115 g m^{-3} will be considered to be the aircraft mean for this subset of data. The FRI and ROL results have lower means than the in situ measurements by 15% and 21%, respectively, but capture the range of observations reasonably well. For R_e, retrieval means show good agreement with the PVM results, with underestimates of 12% and 3% for the FRI and ROL methods, respectively. Again, the range of retrieved droplet sizes is comparable to the range of observed sizes. These comparisons demonstrate that the retrievals produce results that are statistically similar to in situ observations.

b. Technique-to-technique comparisons

The subset of observations to which both the FRI and ROL retrievals were applied provides a dataset for comparing the results of these two methods. Direct comparisons of FRI and ROL retrievals of R_e (Fig. 5a) and LWC (Fig. 5b) show good agreement for R_e smaller than ~10 μm (78% of the data) and LWC less than ~0.25 g m^{-3} (87% of the data), respectively. Above these values, the ROL-derived R_e and LWC approach upper limits for larger values from the FRI retrieval. These limits are due to the approximate reflectivity boundary of −15 dBZ that was used to distinguish liquid clouds from drizzle (Frisch et al. 1995), because, for example, −15 dBZ corresponds to about 14 μm when using the ROL method. The FRI technique does not have the same upper limits because it is not based on reflectivity alone. This comparison suggests that the ROL method may underestimate R_e and LWC for a relatively small subset of cases with large values. The RSD between the FRI and ROL R_e retrievals is low (28%), and the ROL results are biased to be slightly smaller (see Table 4). For LWC (and LWP), the RSD is 72% (76%) and the bias is 14% (8%).

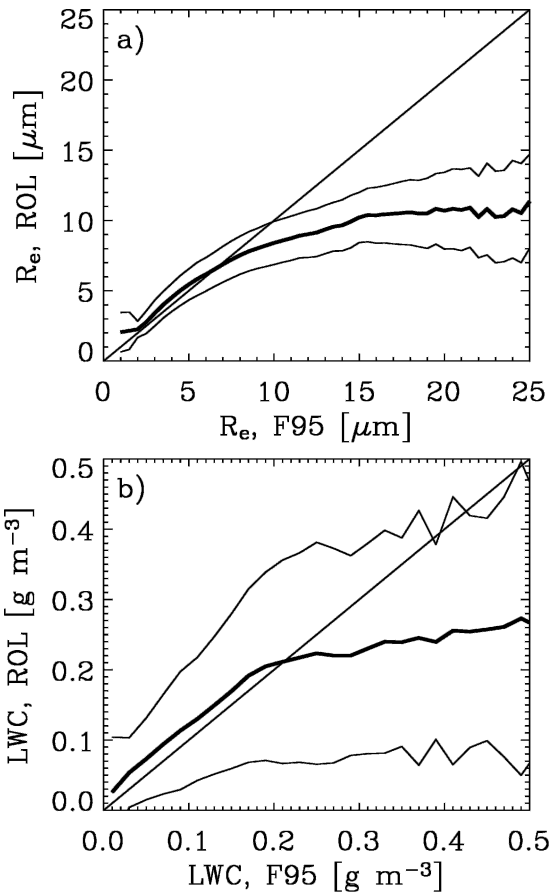

FIG. 5. Comparison of all-liquid cloud (a) R_e and (b) LWC retrieved from the ROL method vs those from the FRI method. The curves are the mean value (thick) surrounded by the standard deviation (thin) of the ROL results in (a) 0.5-μm-wide and (b) 0.02 g m^{-3}–wide bins of the FRI retrieval results.

c. Theoretical uncertainties

Frisch et al. (1995, 1998, 2002) computed theoretical uncertainties based on input errors for the FRI retrieval and an R_e retrieval similar to the ROL method implemented here. These calculations were duplicated using slightly different estimated uncertainties for the parameters of the liquid DSD based on FIRE ACE aircraft observations in all-liquid clouds only [a subset of the data used by Frisch et al. (2002)]. The estimated uncertainties in N_l and σ, based on in situ data, are about 75% and 23%, respectively. The uncertainty in LWP, as inferred from MWR measurements, is assumed to be 25% and the reflectivity uncertainty is as given by Frisch et al. (2002). Based on these values, the theoretical uncertainties in the FRI retrievals of LWC and R_e are 35% and 14%, respectively. For the ROL method, the respective theoretical uncertainties are 48% and 15%.

d. Discussion of liquid retrievals and summary of uncertainties

The largest expected liquid retrieval uncertainties, based on the comparisons presented here, are given in Table 5. Although there can be relatively large uncertainties in some specific cases, the statistical comparison of nearly 8 h of data over 5 days (Fig. 4) reveals reasonably good agreement. These results suggest that the retrievals may produce better results when considered in a statistical manner over longer time periods. This improvement appears to be particularly true for the ROL retrieval method, which fixes N_l based on regional observational statistics. Gultepe and Isaac (1999, 2004) indicate that N_l in fact varies with temperature and aerosol concentrations. Thus, the assumed fixed value may not capture the case-to-case variability but will more likely capture the long-term trend (median) of N_l. For the FRI retrieval, N_l is derived from independent LWP measurements, which leads to its differences from the ROL method. Furthermore, the FRI method overpredicts the number of small N_l cases relative to the FIRE ACE C-130 observations, yielding a median value of 43 cm^{-3}, which is much lower than the in situ observations suggest. Last, the lower sensitivity limit of the radar will lead to a lower limit on all retrieved quantities and an unquantified but small contribution to the overall retrieval uncertainty for both methods.

Together, these analyses suggest that the ROL method, when employed with region-specific coefficients on a long data record, produces statistical results

TABLE 4. Correlation coefficients (corr), relative standard differences (RSD), and biases (bias) between retrieval techniques. RSD and bias are in percent. See text for explanation of retrieval type abbreviations.

	R_e or D_{mean}			LWC or IWC			LWP or IWP		
Retrieval types	Corr	RSD	Bias	Corr	RSD	Bias	Corr	RSD	Bias
FRI–ROL	0.82	28	6	0.59	72	−14	0.49	76	−8
M99–M02	0.68	46	−7	0.61	79	−6	0.67	75	0
M99–ROI	0.82	36	−2	0.77	62	2	0.78	65	14
M02–ROI	0.67	40	6	0.70	73	9	0.79	64	14

TABLE 5. Summary of retrieval uncertainties. For each retrieval method and each parameter the highest determined uncertainties are given based on in situ comparisons and based on relative standard differences from technique intercomparisons.

	LWC or IWC		R_e or D_{mean}	
	In situ	Technique	In situ	Technique
FRI	49%	72%	32%	28%
ROL	47%	72%	32%	28%
M99	64%	79%	27%	46%
M02	100%	79%	30%	46%
ROI	70%	73%	26%	40%

that are similar in accuracy to the multisensor FRI retrieval method. Furthermore, because of the applicability limitations of the FRI method (see section 2c), the ROL method was applied 4 times as often at SHEBA, rendering it most useful for long-term operational cloud monitoring at SHEBA. The distinct advantages of the FRI method are that it is constrained by independent measurements (the MWR-derived LWP) and that it does not require region-specific coefficients.

4. Ice retrieval assessment

a. Comparisons between retrieval and in situ measurements

Ice cloud retrieval comparisons during SHEBA are limited by the dearth of ice clouds sampled by aircraft during FIRE ACE. The measurement errors (e.g., Gayet et al. 2002) and difficulties encountered when processing ice in situ data (Larsen et al. 1998; Baker et al. 2002) have further limited the amount of ice cloud in situ data that are available for retrieval assessments.

The most extensive direct comparison between the ice cloud retrieval techniques assessed here and in situ measurements made during FIRE ACE is described by Matrosov et al. (2002). They discuss a cirrus cloud case study on 28–29 April when the National Research Council of Canada's Convair-580 flew a spiral descent over the SHEBA ice camp. An updated comparison for this case, which incorporates the latest operational version of each retrieval method, showed that the RSD between IWC retrievals and in situ measurements was 64%, 100%, and 70% for the M99, M02, and ROI methods, respectively. The respective RSDs for D_{mean} were 27%, 30%, and 26%. In terms of layer mean properties, the ROI method showed slightly better agreement with in situ measurements than did the other two retrieval methods.

An additional comparison between remote sensing retrievals and C-130 measurements from 2128 to 2206 8 July at SHEBA is shown in Fig. 6. In situ IWC values were derived from an ensemble PSD constructed from separate FSSP, CPI, and 2DC PSDs using the method of Baker et al. (2002) for time periods when the aircraft was within 10 km of the vertical radar beam. The mean and standard deviation of retrieval results over the 20-min time period surrounding the in situ observations are provided for the ROI and M02 methods (the M99 method was not used because of an AERI outage) to give an estimate of the IWC variability over the time period that the aircraft was sampling. Throughout the cloud layer the comparisons are very good, with in situ estimates within the standard deviation of the retrieval measurements at all heights in the cloud. The RSD (and bias) between the mean retrieved IWC values and in situ measurements are 30% (26%) and 27% (17%) for the ROI and M02 methods, respectively. Ice particle sizes are not compared for this case because of uncertainties in computing accurate ice particle characteristic sizes from the ensemble in situ PSD.

b. Technique-to-technique comparisons

The ice cloud retrievals of D_{mean}, IWC, and IWP are compared for cases in which all three retrieval techniques were simultaneously applied. Retrieved values of ice particle D_{mean} (Fig. 7a) show the best agreement among the three techniques for sizes smaller than about 100 μm (71% of the data). At larger sizes both radar-only techniques underestimate D_{mean} when compared with the M99 technique. RSDs between the datasets

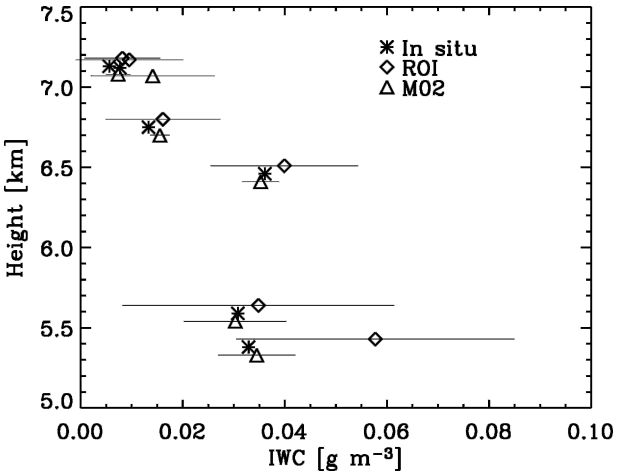

FIG. 6. Comparison of in situ and retrieved IWC from 2128 to 2206 8 Jul 1998. In situ measurements (stars) are horizontal leg averages when the aircraft was within 10 km of the SHEBA site. Radar retrieval results from the ROI (diamonds) and M02 (triangles) methods are expressed as the mean (symbol) and standard deviation (lines) over a 20-min period surrounding the in situ measurements at a given height.

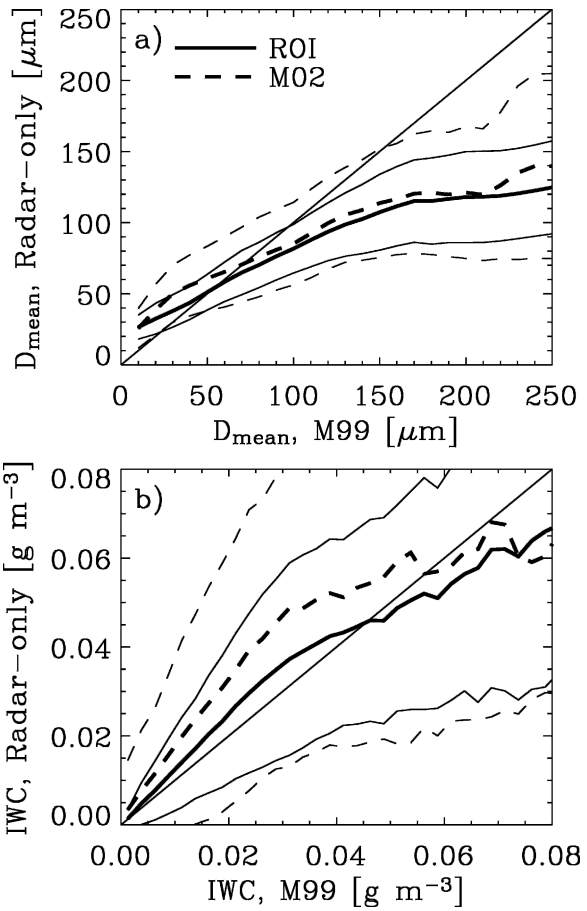

FIG. 7. Comparison of all-ice cloud (a) D_{mean} and (b) IWC retrieved using the ROI (solid) and M02 (dashed) techniques vs those from the M99 technique. The curves are the mean (thick) surrounded by the standard deviation (thin) of the ROI or M02 results in (a) 10-μm-wide and (b) 0.0025 g m^{-3}–wide bins of the M99 retrieval results.

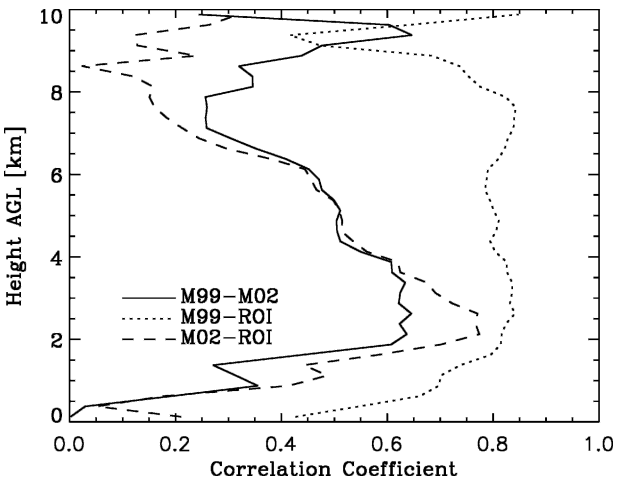

FIG. 8. Correlation coefficient between ice particle size retrievals with height. Height bins of 250 m were used, and the number of points used in the calculations drops off at heights above 8 km.

are 36% and 46% for the M99–ROI and M99–M02 comparisons, respectively (Table 4). The correlation between methods is best in the height range of 2–6 km, with diminishing correlation at higher and lower altitudes (Fig. 8).

Intercomparisons of IWC retrievals show much wider scatter than the D_{mean} comparisons (Fig. 7b), resulting in larger RSDs of 62%–79% among techniques (Table 4). Comparisons of IWP are similar to those for IWC. For both IWC and IWP, the RSD between the ROI and the other methods is less than that between the M99 and M02 methods.

c. *Discussion of ice retrievals and summary of uncertainties*

The expected ice retrieval uncertainties are given in Table 5. As with the liquid retrievals, the RSD between methods is typically larger than the uncertainties inferred from aircraft comparisons, because the RSD combines the uncertainties of both methods. Differences between the M99 and ROI methods are solely due to differences in the specification of the a and b coefficients. However, because the ROI coefficients were statistically derived, in part, from the M99 results, these two methods are similar when considered over a large statistical sample. On the contrary, differences between the reflectivity- and Doppler velocity-based methods are related to the correlation between Z_e and V_z measurements (e.g., Mace et al. 2002). At SHEBA, this correlation decreased with height, likely because of contamination of the V_z measurements from the horizontal winds (see section 2c). An analysis of radiosonde-measured wind speed and direction, along with the known orientation of the radar antenna, revealed that the potential wind contamination increased, in a mean sense, from 0 near the surface to a maximum of about 10 cm s^{-1} at 8 km (similar to Fig. 8). Further study of the variability in the correlation between Z_e and V_z measurements is beyond the scope of this study.

These analyses suggest that the multisensor, multimeasurement techniques discussed here do not provide substantially more accurate results than the empirical power-law retrieval that is implemented with a region-specific, seasonally varying coefficient. For the most-documented case on 28 April, all three methods show a similar D_{mean} uncertainty when compared with in situ measurements and the M99 method shows only slightly better agreement in terms of IWC. The ROI method appears to have better statistical agreement with both the M99 and M02 methods than they do between themselves. Because of the limited set of cloud scenes to which the M99 method can be applied, and its reliance

on two distinct data streams, the ROI method was applied to 7 times as many ice clouds at SHEBA. Furthermore, the off-zenith tilt of the radar coupled with the impact of horizontal winds (section 2c) adds unquantified and variable uncertainty to the M02 retrieval results from SHEBA (this uncertainty can be mitigated when the radar is mounted on a fixed-ground surface). The M02 method also faces limitations under circumstances with larger vertical air motions that are not removed by the 20-min averaging and by cases with ascending velocities. Because of these considerations, the ROI retrieval is best suited for operational cloud monitoring and for capturing the evolution of cloud properties over the course of the annual cycle at SHEBA. The other methods are important for tuning the seasonally varying coefficient used in the ROI method and, at times, provide a moderate improvement in accuracy for selected case studies.

5. Single-phase Arctic cloud properties

a. Cloud-type occurrence

All-liquid, all-ice, and mixed-phase cloud layers were observed in the atmospheric column above SHEBA 19%, 38%, and 41% of the time, respectively. All-liquid clouds were the only cloud layers observed 8% of the time, and all-ice clouds were the only clouds observed 13% of the time. Multilayered cloud scenes containing multiple cloud types were common.

The annual cycles of monthly cloud fraction for each cloud classification type are given in Fig. 9. Over the course of the annual cycle, the all-ice cloud monthly frequency ranged from 23% to 52% and showed no apparent annual cycle trend. All-liquid clouds occurred most frequently from May through September and least frequently from December through April, following the annual cycles of atmospheric temperature and moisture. However, all-liquid clouds did occur ~7% of the time in the cold and dry winter and early spring months. Clouds classified as being mixed phase showed a tendency toward a higher occurrence in the spring and autumn transition seasons, suggesting that the temperatures in these seasons are most able to support the presence of both phases. As with the all-liquid clouds, a significant number of these liquid-containing mixed-phase clouds also occurred in the winter months at SHEBA. Liquid precipitation (drizzle and rain) was observed from May through September, reaching a maximum monthly frequency in the middle of summer, with an annual-averaged frequency of 7%. Snow occurred most frequently in the winter and transition-season months, with an annual mean frequency of 6%.

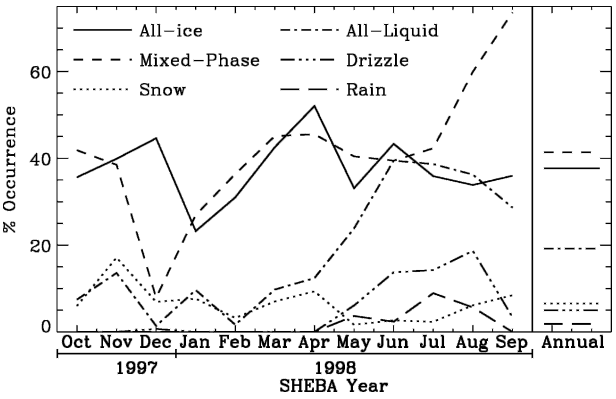

FIG. 9. Annual cycles of monthly cloud-type occurrence. In any given month, the summation of all cloud-type fractions will not necessarily be 100% because of clear-sky time periods and multilayered cloud scenes that contain more than one cloud type.

b. Single-phase cloud microphysical properties

Microphysics results from the radar-only ROL and ROI retrieval methods for all-liquid and all-ice clouds are presented here. These reflectivity-only methods are used because they are most widely applicable, providing both continuity and a large statistical sample (total number of hours are provided in Figs. 10d and 12d, discussed below) that can be used to reveal the annual evolution of cloud properties. As was discussed above, the reflectivity-only methods show a comparable level of statistical uncertainty to the more complex multisensor techniques when applied to a large dataset. For each parameter of interest the following statistics have been computed on a monthly and yearly basis: mean, standard deviation, number of observations, and 5th, 25th, 50th, 75th, and 95th percentiles.

Liquid cloud droplet effective radii show little variation from month to month during the spring and summer but are somewhat smaller in the winter (Fig. 10a). The difference in both mean and median droplet sizes from winter to summer (~25%–30%) is similar to the uncertainty associated with this parameter. Because the distribution of retrieved R_e is roughly normal in shape (Fig. 11a), the annual mean, median, and mode values are all about 6.5 μm. Monthly mean and median values vary between 5 and 7 μm over the course of the year.

Retrieved LWCs also show an annual trend with the smallest values in January and larger LWCs in the summer (Fig. 10b). The difference in monthly means and medians from winter to summer (>100%) is larger than the uncertainty for LWC retrievals, suggesting that this trend is significant. The distribution of retrieved LWCs is exponential in shape (Fig. 11b); the annual mean is 0.10 g m^{-3}, and 95% of the values are below 0.3 g m^{-3}. The annual evolution of retrieved LWP (Fig. 10c) fol-

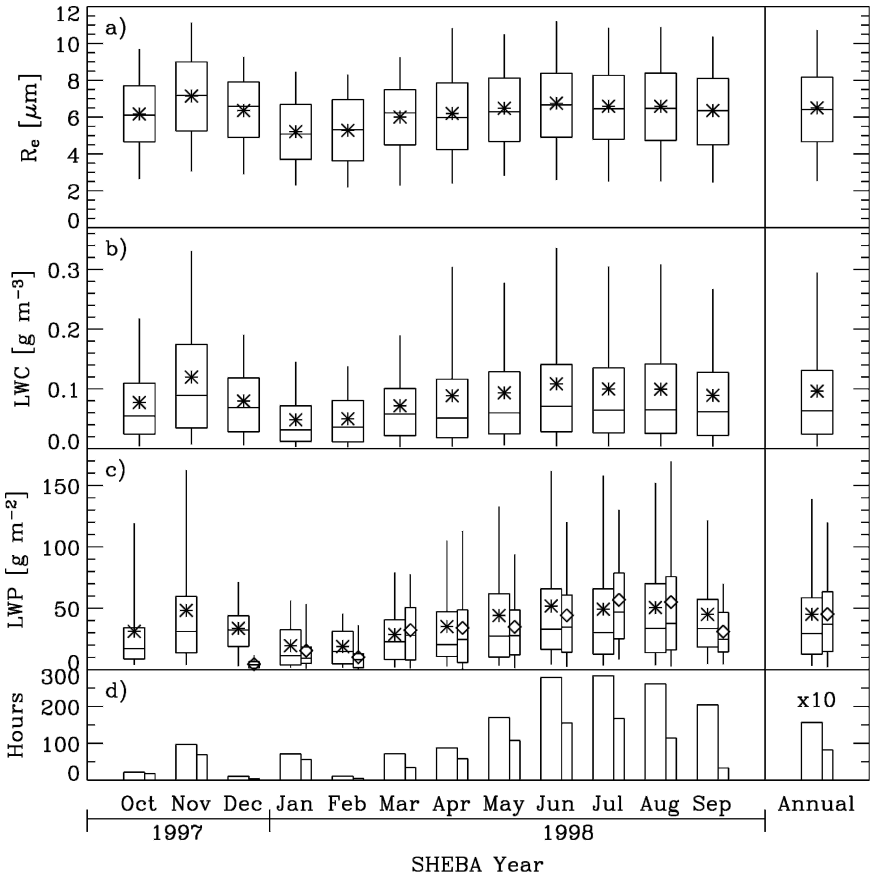

FIG. 10. Monthly and annual statistics of all-liquid cloud (a) droplet effective radius, (b) liquid water content, (c) liquid water path, and (d) hours of occurrence. The box-and-whisker plots provide the 5th, 25th, 50th, 75th, and 95th percentiles of the data, and the mean is given as a symbol. Statistics for the microwave radiometer–derived liquid water path [diamonds in (c)] are also provided; however, fully calibrated MWR data are not available prior to 5 Dec 1997.

lows that of LWC. Winter monthly mean LWPs are ~20 g m^{-2}; summer monthly means reach 50 g m^{-2}. These radar-retrieved values show good agreement in trend, magnitude, and range with the monthly mean, all-liquid cloud LWPs derived from the MWR (diamonds in Fig. 10c). Both methods show an annual-mean all-liquid cloud LWP of ~45 g m^{-2}.

The annual-average-retrieved ice particle D_{mean} is 73 μm; monthly statistics suggest that, on average, the smallest particles occur in the winter and the largest particles occur in the summer (Fig. 12a). This trend may be considered to be significant because the differences in both mean and median size between the February minimum and July maximum are greater than 80%, which is substantially larger than the uncertainty associated with the size retrievals. The distribution of retrieved sizes (Fig. 13a) reveals that 90% of the D_{mean} values are between 20 and 160 μm and that virtually no values are larger than 300 μm.

Retrieved IWCs also show annual variability in the range of observed values (Fig. 12b). While small values of IWC occur in all months (i.e., roughly exponentially distributed data, Fig. 13b), the range of retrieved IWCs is largest in the autumn and smallest in the spring. The monthly mean and median IWCs increase by more than a factor of 4 from the spring to the autumn. The annual mean IWC is 0.014 g m^{-3}, and 95% of IWCs are less than 0.06 g m^{-3}. Total column IWP undergoes a similar annual trend to IWC with the smallest range of values in spring and the largest in autumn (Fig. 12c). The annual mean all-ice cloud IWP is 30 g m^{-2}.

c. *Vertical profiles of cloud microphysical properties*

To examine statistically the vertical distribution of microphysical properties in the clouds observed at SHEBA, retrieved profiles were normalized in height. Vertical profile statistics were calculated for selected

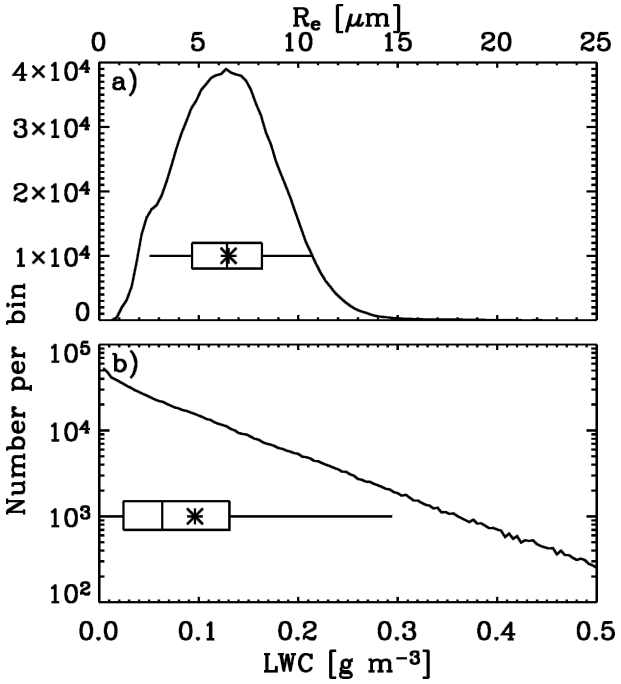

FIG. 11. Annual normalized distributions of retrieved all-liquid cloud (a) droplet effective radius and (b) liquid water content. The box-and-whisker plots summarize the distributions.

single cloud layers that were well developed (i.e., not tenuous or multilayered systems). For consideration here, individual profiles within the designated single-layer cloud regions fulfilled the following criteria: Single cloud-type classification, continuous layer that was fully observed by the radar (i.e., base was above 105 m), and a minimum of 225 m, or five radar range gates, thick. Each profile was normalized in both cloud geometric depth and parameter value. Statistics were then computed on the full set of normalized profiles. For this reason, the mean profiles discussed below do not reach either 0 on the low side or 1 on the high side (which would only be the case if every profile showed the extrema at the same normalized height levels).

The average vertical distribution of microphysical properties within single-layer all-liquid clouds undergoes a moderate annual trend. The largest droplets and LWCs are found at or below the middle of the cloud in the winter months but above the middle of the cloud during the other months of the year (Fig. 14). This trend suggests that the extent to which liquid clouds form through adiabatic ascent may be tied to the seasonal variation of low-level atmospheric stability. Indeed, Arctic temperature inversions are stronger and deeper in the winter (Kahl 1990) causing higher atmospheric stability and subsequently less adiabatic lifting in cloud formation.

All retrieved liquid cloud microphysical properties, in an annually averaged sense, increase from the cloud base up to about 60% of the average cloud depth from the base, at which height the parameters decrease up to the cloud top (e.g., Fig. 14). This shape suggests a semiadiabatic liquid water profile with a relatively large layer of mixing/entrainment near the cloud top. Pinto et al. (2001) and Lawson et al. (2001) observed similar low-level cloud profile shapes from aircraft measurements made during the autumn over the Beaufort Sea and the spring–summer over the SHEBA camp, respectively, as well as observing deep cloud-top mixing in some cases.

There is no clear annual trend to the vertical distribution of ice microphysical properties within single-layer ice clouds. Figure 15 shows the annual-average normalized profiles of retrieved IWC and D_{mean}. The average level of largest particle sizes and highest IWCs is at one-forth of the cloud depth from the base, reflecting the growth of ice particles as they fall from the cloud top and their rapid sublimation near cloud base. These profile shapes are similar to the all-ice cloud profiles observed at many midlatitude locations by Matrosov (1997).

6. Summary and conclusions

An operational suite of ground-based remote sensor cloud microphysics retrievals is described and assessed using 1 yr of observations from the SHEBA program that included episodic aircraft measurements from the FIRE ACE experiment. The retrieval suite combines multiple ground-based sensors and radiosondes to classify cloud scenes as all ice, all liquid, mixed phase, or precipitation. To each of these cloud scene types, one or more retrieval methods are applied. Here, only the single-phase liquid and ice cloud retrieval methods are assessed using in situ comparisons, technique intercomparisons, and analytical error analyses to provide uncertainty estimates for retrieved cloud properties (summarized in Table 5). With moderate differences between methods, liquid cloud R_e and LWC can be retrieved with uncertainties of no worse than 32% and 49%–72%, respectively. Ice cloud D_{mean} and IWC can be retrieved with uncertainties of 26%–46% and 62%–100%, respectively. These uncertainties can be considered representative for the application of these specific retrievals to SHEBA observations. However, further study is necessary to determine if these uncertainties are representative for other locations.

The assessment presented here indicates that, from a long-term statistical point of view, region-specific radar-only retrieval methods are best suited for monitor-

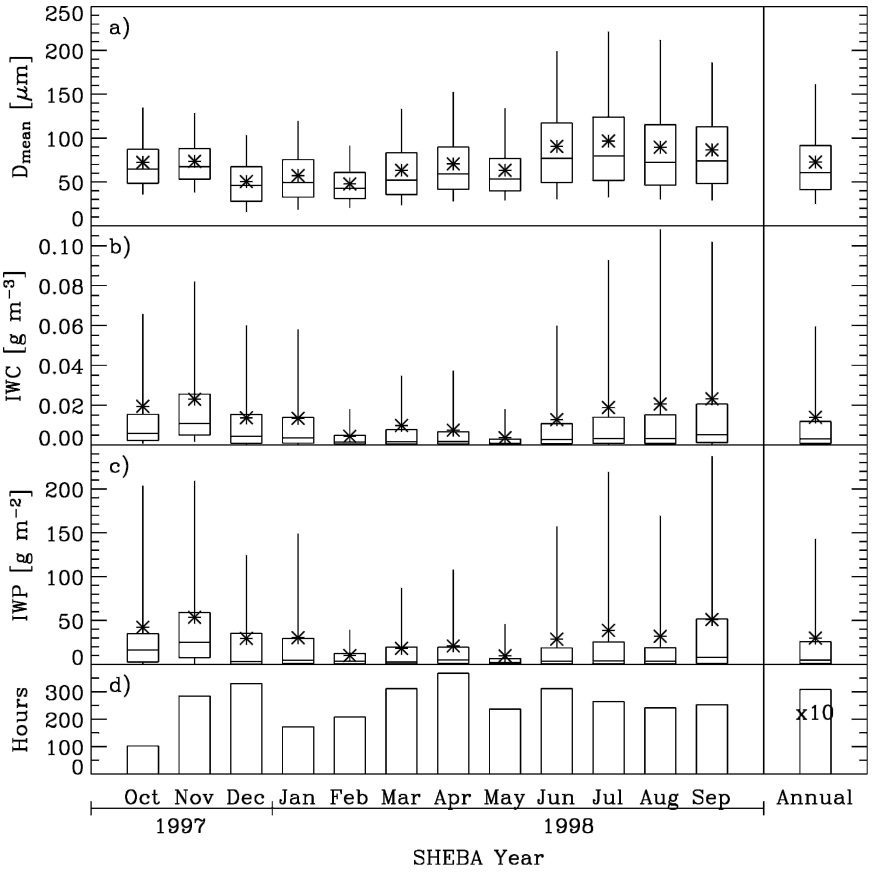

FIG. 12. As in Fig. 10, but representing all-ice cloud (a) D_{mean}, (b) IWC, (c) IWP, and (d) hours of occurrence.

ing the evolution of Arctic cloud properties. The multisensor, multimeasurement methods discussed here are constrained by more measurements and thus may show a moderate improvement in accuracy over the radar-only methods for some case studies. For the ice retrievals, the multimeasurement methods are also needed to derive a seasonally varying, region-specific coefficient for the radar-only retrieval. However, these multimeasurement techniques (which are similar to methods proposed by others) suffer from various limitations that render them applicable to relatively few cases. On the other hand, the radar-only methods are widely applicable with few limitations and were therefore applied to 4 times as many liquid cloud cases and 7 times as many ice cloud cases during the year of observations at SHEBA. Once region- and season-specific coefficients were determined, the statistical uncertainty of these radar-only retrievals, when applied to 1 yr of data, was comparable to that of the multimeasurement methods. Thus, the radar-only methods produced a nearly as accurate, yet more detailed and extensive, cloud properties dataset with which to monitor the seasonal evolution of Arctic cloud microphysical properties at SHEBA.

This operational retrieval framework and, specifically, the radar-only retrieval methods have been used to obtain important information on the annual evolution of Arctic cloud presence and microphysical properties. During the SHEBA year, clouds were classified as all liquid, all ice, and mixed phase for 19%, 38%, and 41% of the time, respectively. All-liquid clouds predominantly occurred in the summer; ice clouds occurred throughout the year. Mixed-phase clouds were most frequent in the spring and autumn transition seasons.

Liquid cloud retrieval results showed some seasonal variation in R_e, LWC, and LWP, with the smallest values in the dry winter and the largest values in the relatively moist summer. The annual-average properties are $R_e = 6.5$ μm, LWC = 0.10 g m^{-3}, and LWP = 45 g m^{-2}. Liquid clouds at SHEBA, on average, showed R_e and LWC growing from the cloud base up to about 60% of the cloud depth from the base.

Ice cloud particle sizes are, on average, largest in the

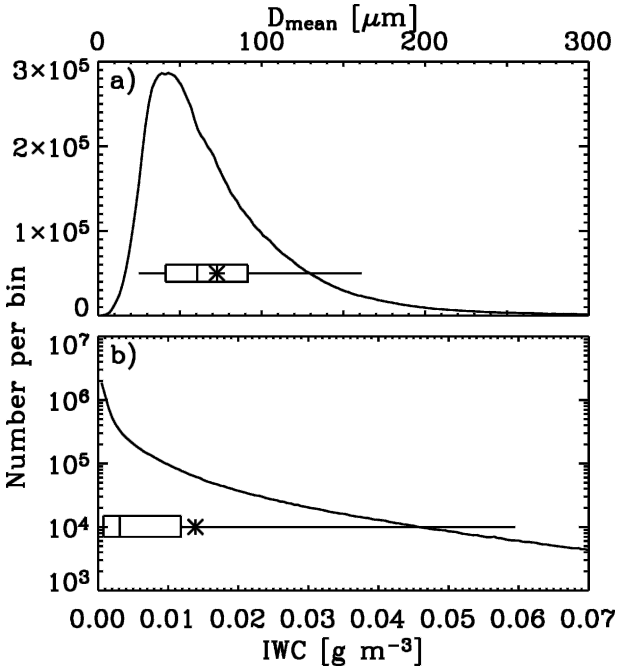

FIG. 13. As in Fig. 11, but representing all-ice cloud (a) D_{mean} and (b) IWC.

summer and smallest in the winter, while IWC and IWP show the largest range of values in the autumn. The annual-average ice cloud properties are $D_{\text{mean}} = 73$ μm, IWC = 0.014 g m^{-3}, and IWP = 30 g m^{-2}. Average vertical profiles of ice cloud properties show the largest sizes and IWCs at one-fourth of the cloud depth from the cloud base, which demonstrates the growth of cloud particles as they fall and rapid sublimation in a thin layer near the cloud base.

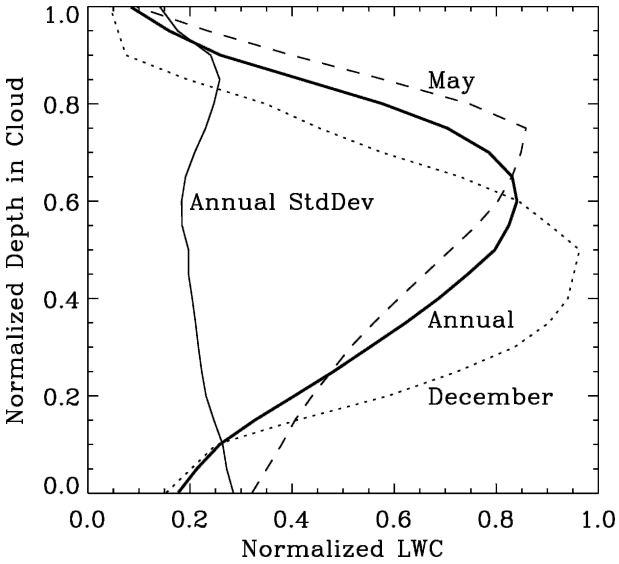

FIG. 14. Annual mean, normalized profiles of retrieved all-liquid cloud LWC (thick) and the profile of standard deviation (thin). Monthly mean profiles are also provided for Dec and May.

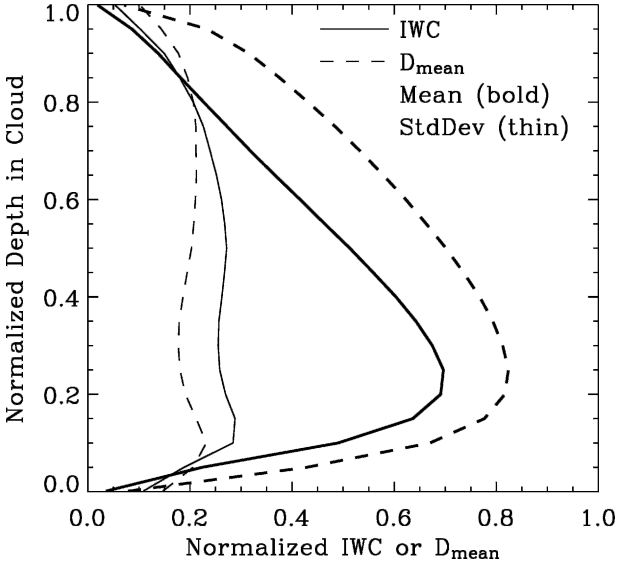

FIG. 15. Annual mean, normalized profiles of retrieved IWC and D_{mean} (thick curves) and the profiles of standard deviation (thin curves).

The data presented here are useful in a variety of ways. First, they provide an initial look at the annual mean and variability of various Arctic cloud microphysical properties. Past measurements of these quantities have been restricted to short time periods during Arctic daylight, with few measurements during the dark and cold Arctic winter. Second, these results are useful for comparison with satellite observations. The cloud-type identification discussed in section 2b can be used to validate satellite cloud scene identification over the SHEBA region, and the microphysical statistics provide a base with which to compare satellite cloud retrievals. Furthermore, the vertical profiles of microphysical parameters can provide useful insight into how differences in viewing orientation (i.e., surface vs space) influence the retrieval of bulk cloud parameters. These data also can be used to assess model-produced cloud fields. Comparisons of total cloud water and precipitation budgets from SHEBA have already revealed shortcomings in phase partitioning in a single-column model (Morrison et al. 2003).

This retrieval assessment and the subsequent cloud-property results have been limited to a subset of the available radar-based cloud retrieval methods developed at the NOAA Environmental Technology Laboratory. In future work on the topic, a broader assessment including more techniques from a variety of sources (e.g., Dong et al. 1997; Mace et al. 1998; Dono-

von and van Lammeren 2001; McFarlane et al. 2002; Turner 2005) will be useful for insuring the mutual consistency of remote sensing cloud retrievals and for decreasing the operational uncertainty associated with remotely deriving cloud properties.

Acknowledgments. This work was supported by the NSF SHEBA (OPP-9701730 and 0084257), the NASA FIRE ACE (L64205D), the NASA EOS Validation (S-97895-F), NASA ISCCP, and NOAA SEARCH programs. Microwave and IR radiometer data were obtained from the Atmospheric Radiation Measurement Program sponsored by the U.S. Department of Energy. Radiosonde data were obtained from the University of Washington Applied Physics Laboratory (UW APL). Aircraft data were obtained from the National Center for Atmospheric Research, B. Baker, P. Lawson, and P. Zuidema are gratefully acknowledged for providing the in situ ice microphysical data, and S. Frisch and G. Feingold provided valuable insight into liquid cloud retrievals. SHEBA was greatly aided by the logistics team from the UW APL and the crew of the Canadian Coast Guard Ship *Des Grosseilliers*.

REFERENCES

Atlas, D., S. Y. Matrosov, A. J. Heymsfield, M.-D. Chou, and D. B. Wolff, 1995: Radar and radiation properties of ice clouds. *J. Appl. Meteor.,* **34,** 2329–2345.

Baker, B., C. Schmitt, P. Lawson, and D. Mitchell, 2002: Further analysis and improvements of ice crystal mass-size relationships. Preprints, *11th Conf. on Cloud Physics*, Ogden, UT, Amer. Meteor. Soc., CD-ROM, P2.15.

Brown, P. R. A., and P. N. Francis, 1995: Improved measurements of the ice water content in cirrus using a total-water probe. *J. Atmos. Oceanic Technol.,* **12,** 410–414.

Curry, J. A., and Coauthors, 2000: FIRE Arctic Clouds Experiment. *Bull. Amer. Meteor. Soc.,* **81,** 5–29.

Dong, X., T. P. Ackerman, E. E. Clothiaux, P. Pilewskie, and Y. Han, 1997: Microphysical and radiative properties of boundary layer stratiform clouds deduced from ground-based measurements. *J. Geophys. Res.,* **102,** 23 829–23 843.

——, P. Minnis, T. P. Ackerman, E. E. Clothiaux, G. G. Mace, C. N. Long, and J. C. Liljegren, 2000: A 25-month database of stratus cloud properties generated from ground-based measurements at the ARM SGP site. *J. Geophys. Res.,* **105,** 4529–4537.

——, ——, G. G. Mace, W. L. Smith Jr., M. Poellot, R. T. Marchand, and A. D. Rapp, 2002: Comparison of stratus cloud properties deduced from surface, GOES, and aircraft data during the March 2000 ARM cloud IOP. *J. Atmos. Sci.,* **59,** 3265–3284.

Donovon, D. P., and A. C. A. P. van Lammeren, 2001: Cloud effective particle size and water content profile retrievals using combined lidar and radar observations, 1. Theory and examples. *J. Geophys. Res.,* **106,** 27 425–27 448.

Fox, N. I., and A. J. Illingworth, 1997: The retrieval of stratocumulus cloud properties by ground-based cloud radar. *J. Appl. Meteor.,* **36,** 485–492.

Frey, R. A., B. A. Baum, W. P. Menzel, S. A. Ackerman, C. C. Moeller, and J. D. Spinhirne, 1999: A comparison of cloud top heights computed from airborne lidar and MAS radiance data using CO_2 slicing. *J. Geophys. Res.,* **104,** 24 547–24 555.

Frisch, A. S., C. W. Fairall, and J. B. Snider, 1995: Measurements of stratus cloud and drizzle parameters in ASTEX with a Ka-band Doppler radar and microwave radiometer. *J. Atmos. Sci.,* **52,** 2788–2799.

——, G. Feingold, C. W. Fairall, T. Uttal, and J. B. Snider, 1998: On cloud radar and microwave radiometer measurements of stratus cloud liquid water profiles. *J. Geophys. Res.,* **103,** 23 195–23 197.

——, M. D. Shupe, I. Djalalova, G. Feingold, and M. Poellot, 2002: The retrieval of stratus cloud droplet effective radius with cloud radars. *J. Atmos. Oceanic Technol.,* **19,** 835–842.

Gayet, J.-F., and Coauthors, 2002: Quantitative measurement of the microphysical and optical properties of cirrus clouds with four different in situ probes: Evidence of small ice crystals. *Geophys. Res. Lett.,* **29,** 2230, doi:10.1029/2001GL014342.

Gultepe, I., and G. Isaac, 1999: Scale effects on averaging of cloud droplet and aerosol number concentrations: Observations and models. *J. Climate,* **12,** 1268–1279.

——, and ——, 2004: Aircraft observations of cloud droplet number concentration: Implications for climate studies. *Quart. J. Roy. Meteor. Soc.,* **130,** 2377–2390.

——, ——, D. Hudak, R. Nissen, and J. W. Strapp, 2000: Dynamical and microphysical characteristics of Arctic clouds during BASE. *J. Climate,* **13,** 1225–1254.

Hobbs, P. V., and A. L. Rangno, 1998: Microstructures of low and middle-level clouds over the Beaufort Sea. *Quart. J. Roy. Meteor. Soc.,* **124,** 2035–2071.

Hogan, R. J., A. J. Illingworth, E. J. O'Connor, and J. P. V. Poiares Baptista, 2003: Characteristics of mixed-phase clouds, Part II: A climatology from ground-based lidar. *Quart. J. Roy. Meteor. Soc.,* **129,** 2117–2134.

Intrieri, J. M., M. D. Shupe, T. Uttal, and B. J. McCarty, 2002: An annual cycle of Arctic cloud characteristics observed by radar and lidar at SHEBA. *J. Geophys. Res.*, **107,** 8030, doi:10.1029/2000JC000423.

Kahl, J. D., 1990: Characteristics of the low-level temperature inversion along the Alaskan Arctic coast. *Int. J. Climatol.,* **10,** 537–548.

Knuteson, R. O., and Coauthors, 2004: Atmospheric Emitted Radiance Interferometer. Part I: Instrument design. *J. Atmos. Oceanic Technol.,* **21,** 1763–1776.

Larsen, H., J.-F. Gayet, G. Febvre, H. Chepfer, and G. Brogniez, 1998: Measurement errors in cirrus cloud microphysical properties. *Ann. Geophys.,* **16,** 266–276.

Laursen, K., cited 1998: Data quality summary: Surface Heat Budget of the Arctic Ocean (SHEBA). NCAR RAF Project 8-101. [Available online at raf.atd.ucar.edu/Projects/SHEBA/sheba_dqsumm.html.]

Lawson, P., B. A. Baker, C. G. Schmitt, and T. L. Jensen, 2001: An overview of microphysical properties of Arctic clouds observed in May and July 1998 during FIRE ACE. *J. Geophys. Res.,* **106,** 14 989–15 014.

Liao, L., and K. Sassen, 1994: Investigation of relationships between Ka-band radar reflectivity and ice and liquid water contents. *Atmos. Res.,* **34,** 231–248.

Liu, C.-L., and A. J. Illingworth, 2000: Toward more accurate retrievals of ice water content from radar measurements of clouds. *J. Appl. Meteor.,* **39,** 1130–1146.

Lohnert, U., S. Crewell, C. Simmer, and A. Macke, 2001: Profiling cloud liquid water by combining active and passive micro-

wave measurements with cloud model studies. *J. Atmos. Oceanic Technol.,* **18,** 1354–1366.

Mace, G. G., T. P. Ackerman, P. Minnis, and D. F. Young, 1998: Cirrus layer microphysical properties derived from surface-based millimeter radar and infrared interferometer data. *J. Geophys. Res.,* **103,** 207–216.

——, A. J. Heymsfield, and M. R. Poellot, 2002: On retrieving the microphysical properties of cirrus cloud using the moments of the millimeter-wavelength Doppler spectrum. *J. Geophys. Res.,* **107,** 4815, doi:10.1029/2001JD001308.

Matrosov, S. Y., 1997: Variability of microphysical parameters in high-altitude ice clouds: Result of the remote sensing method. *J. Appl. Meteor.,* **36,** 633–648.

——, 1999: Retrievals of vertical profiles of ice cloud microphysics from radar and IR measurements using tuned regressions between reflectivity and cloud parameters. *J. Geophys. Res.,* **104,** 16 741–16 753.

——, T. Uttal, J. B. Snider, and R. A. Kropfli, 1992: Estimation of ice cloud parameters from ground-based infrared radiometer and radar measurements. *J. Geophys. Res.,* **97,** 11 567–11 574.

——, A. V. Korolev, and A. J. Heymsfield, 2002: Profiling cloud ice mass and particle characteristic size from Doppler radar measurements. *J. Atmos. Oceanic Technol.,* **19,** 1003–1018.

——, M. D. Shupe, A. J. Heymsfield, and P. Zuidema, 2003: Ice cloud optical thickness and extinction estimates from radar measurements. *J. Appl. Meteor.,* **42,** 1584–1597.

McFarlane, S. A., K. F. Evans, and A. S. Ackerman, 2002: A Bayesian algorithm for the retrieval of liquid water cloud properties from microwave radiometer and millimeter radar data. *J. Geophys. Res.*, **107,** 4317, doi:10.1029/2001JD001011.

Miles, N. L., J. Verlinde, and E. E. Clothiaux, 2000: Cloud droplet size distributions in low-level stratiform clouds. *J. Atmos. Sci.,* **57,** 295–311.

Moran, K. P., B. E. Martner, M. J. Post, R. A. Kropfli, D. C. Welsh, and K. B. Widener, 1998: An unattended cloud-profiling radar for use in climate research. *Bull. Amer. Meteor. Soc.,* **79,** 443–455.

Morrison, H., M. D. Shupe, and J. A. Curry, 2003: Modeling clouds observed at SHEBA using a bulk microphysics parameterization implemented into a single-column model. *J. Geophys. Res.,* **108,** 4255, doi:10.1029/2002JD002229.

Pinto, J. O., J. A. Curry, and J. M. Intrieri, 2001: Cloud–aerosol interactions during autumn over the Beaufort Sea. *J. Geophys. Res.,* **106,** 15 077–15 097.

Rossow, W. B., A. W. Walker, and L. C. Garder, 1993: Comparisons of ISCCP and other cloud amounts. *J. Climate,* **6,** 2394–2418.

Sassen, K., 1984: Deep orographic cloud structure and composition derived from comprehensive remote sensing measurements. *J. Climate Appl. Meteor.,* **23,** 568–583.

——, 1987: Ice cloud content from radar reflectivity. *J. Climate Appl. Meteor.,* **26,** 1050–1053.

——, Z. Wang, V. I. Khvorostyanov, G. L. Stephens, and A. Bennedetti, 2002: Cirrus cloud ice water content radar algorithm evaluation using an explicit cloud microphysical model. *J. Appl. Meteor.,* **41,** 620–628.

Shupe, M. D., T. Uttal, S. Y. Matrosov, and A. S. Frisch, 2001: Cloud water contents and hydrometeor sizes during the FIRE-Arctic Clouds Experiment. *J. Geophys. Res.,* **106,** 15 015–15 028.

——, P. Kollias, S. Y. Matrosov, and T. L. Schneider, 2004: Deriving mixed-phase cloud properties from Doppler radar spectra. *J. Atmos. Oceanic Technol.,* **21,** 660–670.

——, S. Y. Matrosov, and T. Uttal, 2005: Arctic mixed-phase cloud properties derived from surface-based sensors at SHEBA. *J. Atmos. Sci.,* in press.

Stephens, G. L., and Coauthors, 2002: The CloudSat Mission and the A-Train: A new dimension of space-based observations of clouds and precipitation. *Bull. Amer. Meteor. Soc.,* **83,** 1771–1790.

Turner, D. D., 2005: Arctic mixed-phase cloud properties from AERI-lidar observations: Algorithm and results from SHEBA. *J. Appl. Metoer.,* **44,** 427–444.

Uttal, T., and Coauthors, 2002: Surface Heat Budget of the Arctic Ocean. *Bull. Amer. Meteor. Soc.,* **83,** 255–275.

Wang, Z., and K. Sassen, 2002: Cirrus cloud microphysical property retrieval using lidar and radar measurements. Part I: Algorithm description and comparisons with in situ data. *J. Appl. Meteor.,* **41,** 218–229.

Westwater, E. R., Y. Han, M. D. Shupe, and S. Y. Matrosov, 2001: Analysis of integrated cloud liquid and precipitable water vapor retrievals from microwave radiometers during SHEBA. *J. Geophys. Res.,* **106,** 32 019–32 030.

Wielicki, B. A., and L. Parker, 1992: On the determination of cloud cover from satellite sensors: The effect of sensor spatial resolution. *J. Geophys. Res.,* **97,** 12 799–12 823.